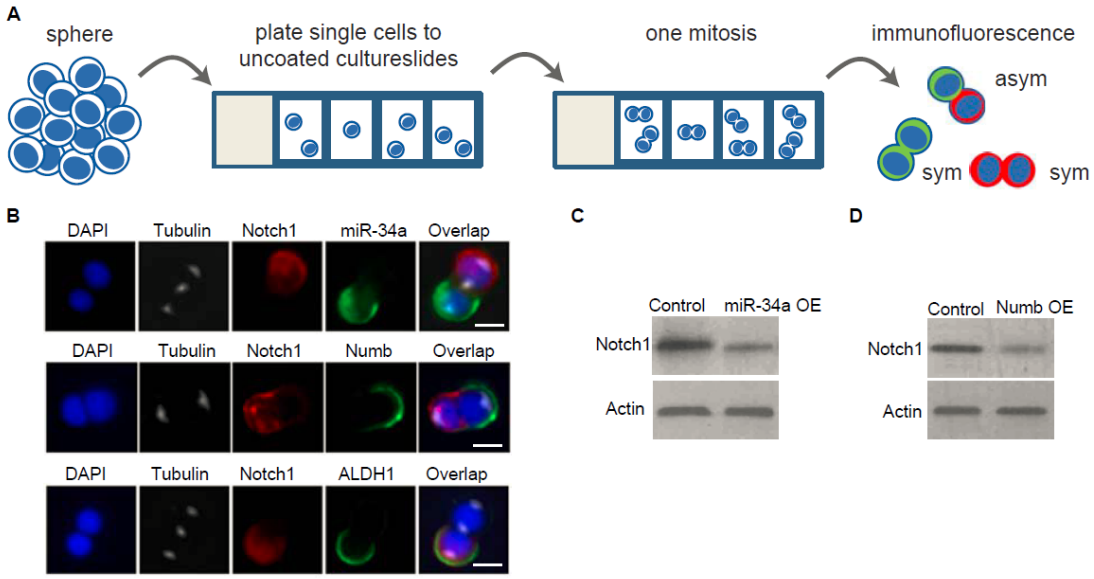

Figure S1. Asymmetric distribution of Notch-targeting miR-34a and Numb during CCSC division. Related to Figure 1.

(**A**) Schematic illustration of the pair-cell assay. (**B**) Representative images of pair-cell assay with staining for miR-34a (green) and Notch1 (red), Numb (green) and Notch1 (red), and ALDH1 (green) and Notch1 (red). Tubulin staining indicates dividing pairs in telophase. (**C** and **D**) Western blot of Notch1 levels with ectopic miR-34a (B) or Numb (C) expression. Scale bar, 8μm.

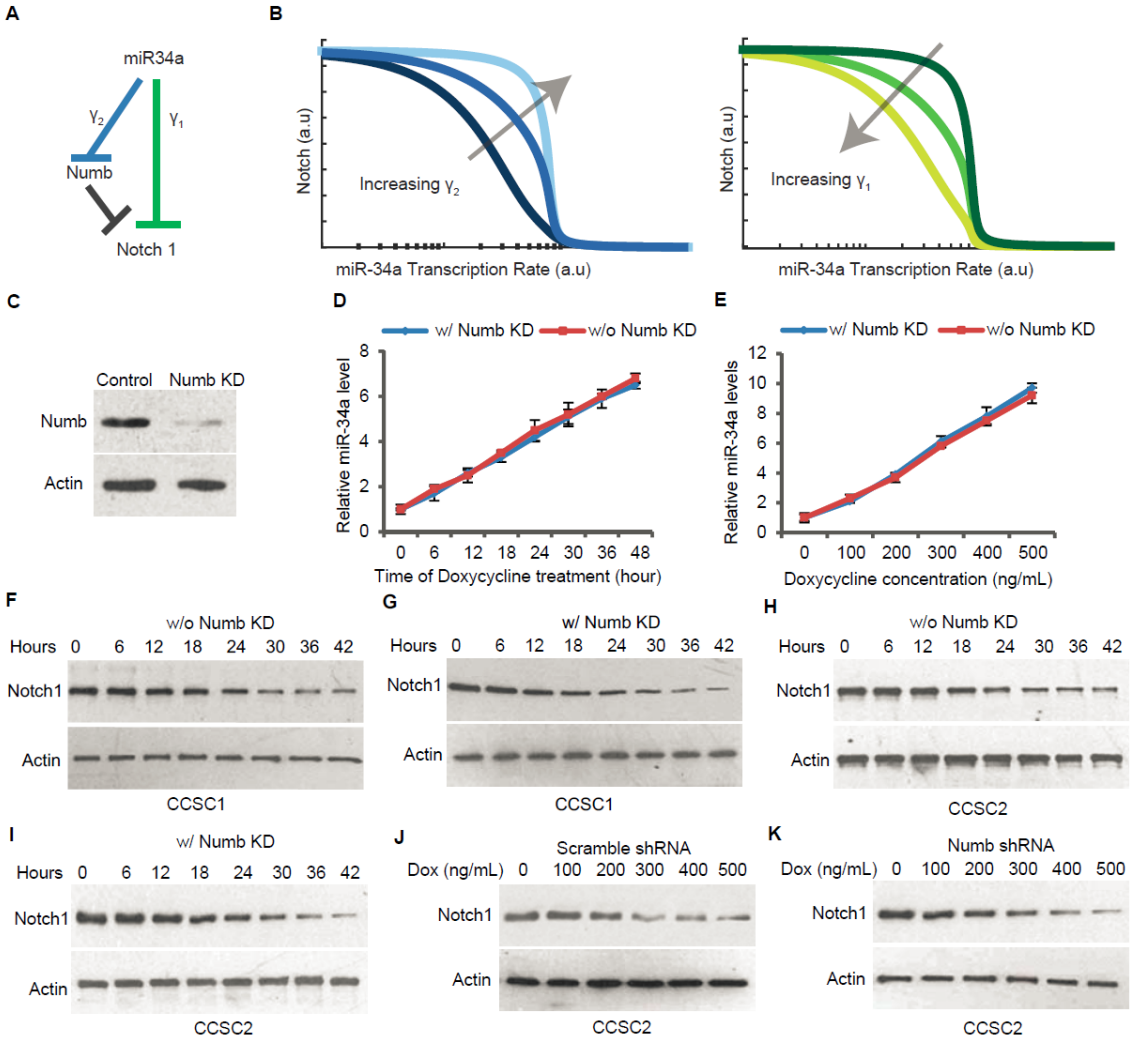

Figure S2. IFFL generates a robust Notch switch. Related to Figures 2 and 3.

(A) Schematic of the IFFL. **(B)** Computational simulation shows the transition (threshold and slope) of the IFFL switch is influenced by the strength of miR-34a suppression of Notch (γ_1) and Numb (γ_2). (**C**) Western blot showing shRNA knockdown of Numb in CCSCs. (**D**) Time-series RT-qPCR measurements of induced miR-34a levels after addition of Doxycycline. (**E**) RT-qPCR measurements of miR-34a levels induced by different Doxycycline concentrations. (**F** and **G**) Time-series Western blot measurements of Notch1 levels without (F) or with (G) Numb knockdown after miR-34a expression in

CCSC1 was induced by 400ng/ml Doxycycline. (**H** and **I**) Time-series Western blot measurements of Notch1 levels without (H) or with (I) Numb knockdown after miR-34a expression in CCSC2 was induced by 400ng/ml Doxycycline. **(J** and **K)** Western blots of Notch levels in scramble shRNA (J) and Numb shRNA (K) infected CCSC2 spheres with incremental mir-34a induction by Doxycycline.

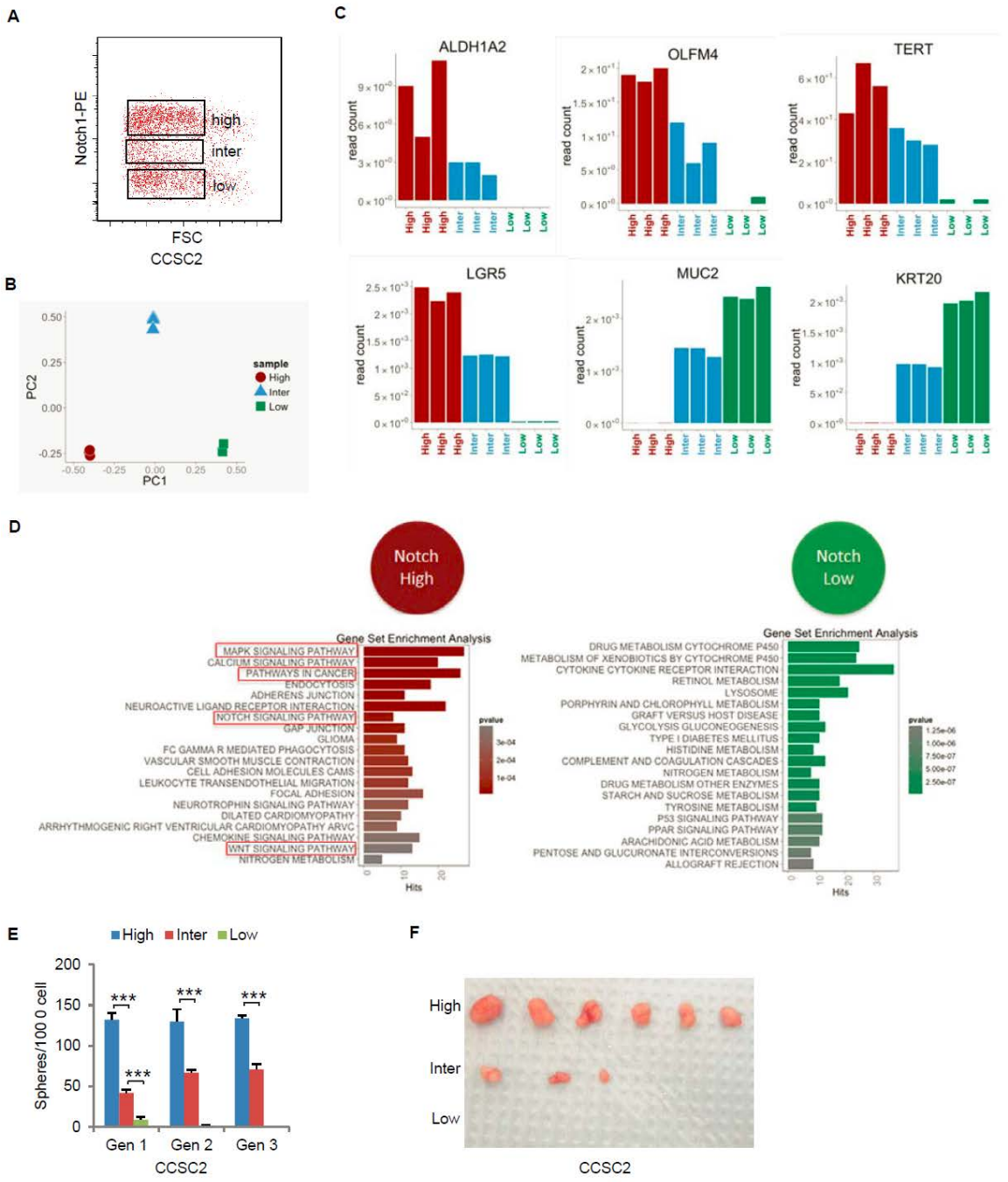

Figure S3. Characterizations of Notch intermediate population in CCSCs generated by Numb knockdown. Related to Figure 4.

(**A**) FACS plot showing Notch^{high}, Notch^{inter}, and Notch^{low} subpopulations of Numb knockdown CCSC2 sphere cells, treated with 200ng/ml Doxycycline. (**B**) Principle

component analysis (PCA) of transcriptomic profiles of Notch^{high}, Notch^{inter}, and Notch^{low} cells. (**C**) Marker expression in Notch^{high}, Notch^{inter}, and Notch^{low} cells. (**D**) Pathways identified by Gene Set Enrichment Analysis (GSEA). (**E**) Serial Sphere propagation of Notch^{high}, Notch^{inter}, and Notch^{low} cells isolated from Numb Knockdown CCSC2 sphere cells. Gen, generation. (**F**) Tumor images showing tumorigenic capability of transplanted Notch^{high}, Notch^{inter}, and Notch^{low} cells. Error bars denote s.d. of triplicates. ***, $p<0.001$. p-value was calculated based on Student's t-test.

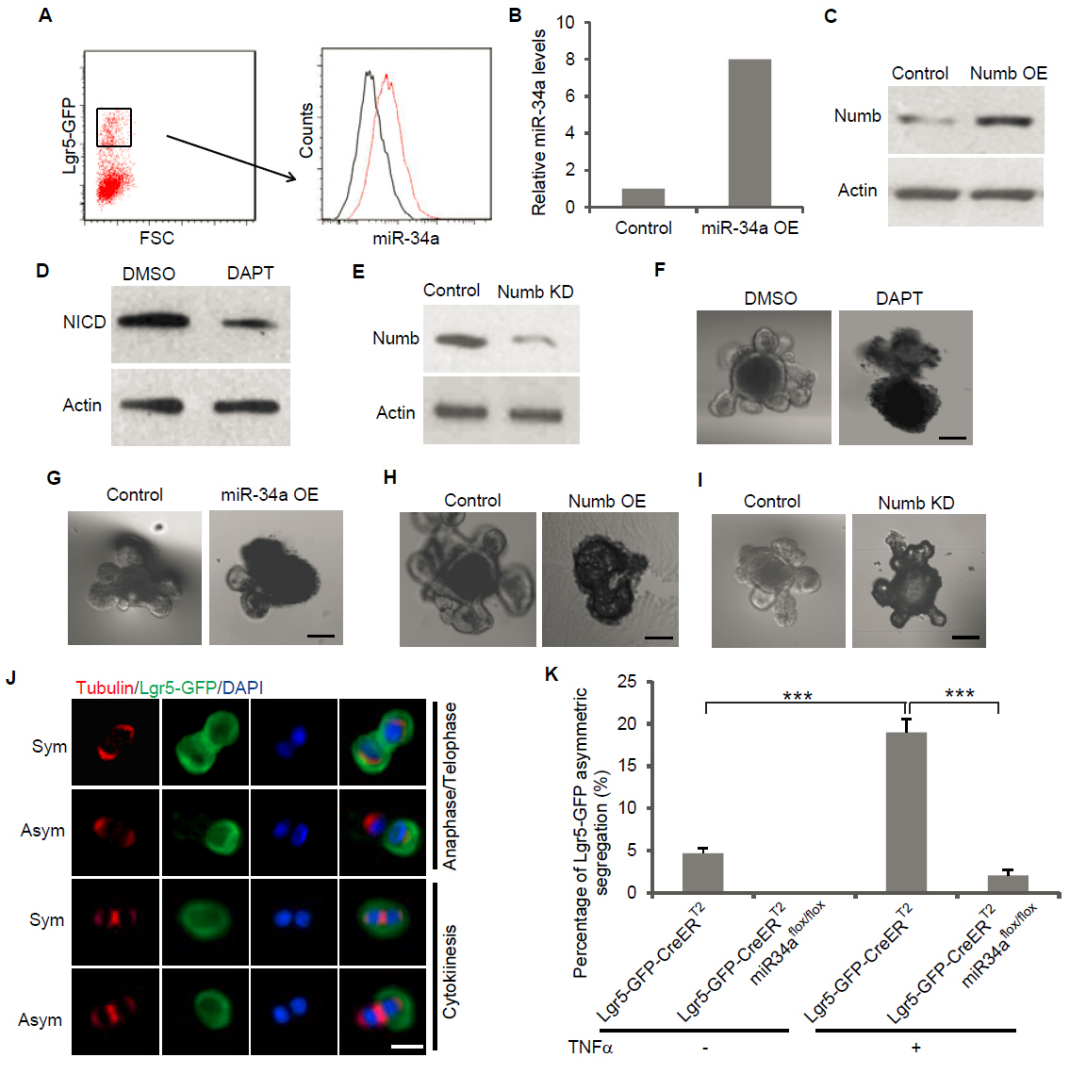

Figure S4. Perturbation of Notch signaling and asymmetric division in mouse intestinal organoids. Related to Figure 5.

(**A**) miR-34a expression in Lgr5-GFP+ cells by FACS with miR-34a FISH probes. (**B**) RT-qPCR showing ectopic miR-34 expression. (**C**) Western blot showing ectopic Numb expression. (D) Western blot showing inhibition of Notch by DAPT. (**E**) Western blot showing Numb knockdown efficiency. (**F-I**) Representative images of organoids with DAPT treatment (F), ectopic miR-34a (G) or Numb (H) expression, and with Numb knockdown (I). (**J**) Representative images of symmetric and asymmetric division of

Lgr5-GFP ISCs in intestinal organoids. Tubulin staining indicates stages of mitosis. The anaphase/telophase images were taken from FACS-sorted Lgr5-GFP+ doublets that were fixed and stained immediately without recovery. The cytokinesis images were taken from the pair-cell assay. Scale bar, 8μm. (**K**) Frequency of asymmetric division of Lgr5-GFP stem cells from *Lgr5-EGFP-CreER*^{T2} and *Lgr5-EGFP-CreER*^{T2}*/miR-34a*$^{flox/flox}$ intestinal organoids with or without TNFα treatment. Error bars denote s.d. of triplicates. ***, $p<0.001$. p-value was calculated based on Student's t-test.

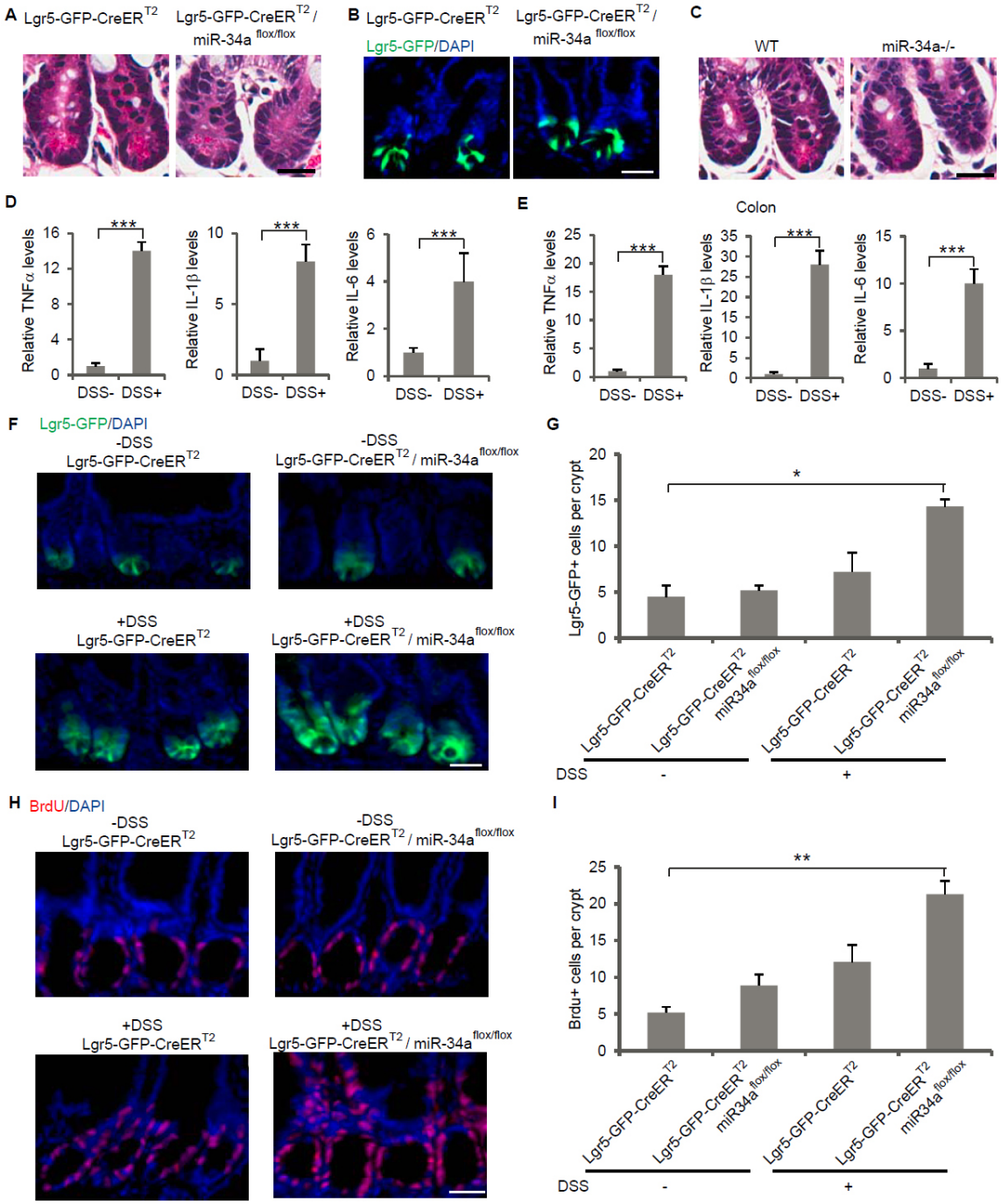

Figure S5. Loss of miR-34a increases DSS-induced proliferation in mouse intestinal crypts. Related to Figure 7.

(**A** and **B**) H&E staining (A) and immunofluorescence (B) of intestinal crypts from *Lgr5-EGFP-CreER^{T2}* and *Lgr5-EGFP-CreER^{T2}/miR-34a$^{flox/flox}$* transgenic mice after

Tamoxifen induction. No obvious phenotypes in terms of morphology or Lgr5-GFP (green) ISCs were observed. (**C**) H&E staining of intestinal crypts from wild type and miR-34a whole-body knockout mice. (**D**) RT-qPCR showing TNFα, IL-1β and IL-6 expression in mouse intestine. (**E**) RT-qPCR showing TNFα, IL-1β and IL-6 expression in mouse colon. (**F** and **G**) Representative images (F) and quantification (G) of intestinal crypts from *Lgr5-EGFP-CreER^{T2}* and *Lgr5-EGFP-CreER^{T2}/miR-34a$^{flox/flox}$* mice administrated with DSS or plain water. DSS treatment followed by recovery increased Lgr5-GFP ISCs in the intestine. (**H** and **I**) Representative images (H) and quantification (I) of cell proliferation identified by the BrdU incorporation assay in mouse intestine. DSS and loss-of miR-34a increases proliferation. Scale bar, 50μm. *, $p<0.05$; **, $p<0.001$; ***, $p<0.001$. p-value was calculated based on Student's t-test.

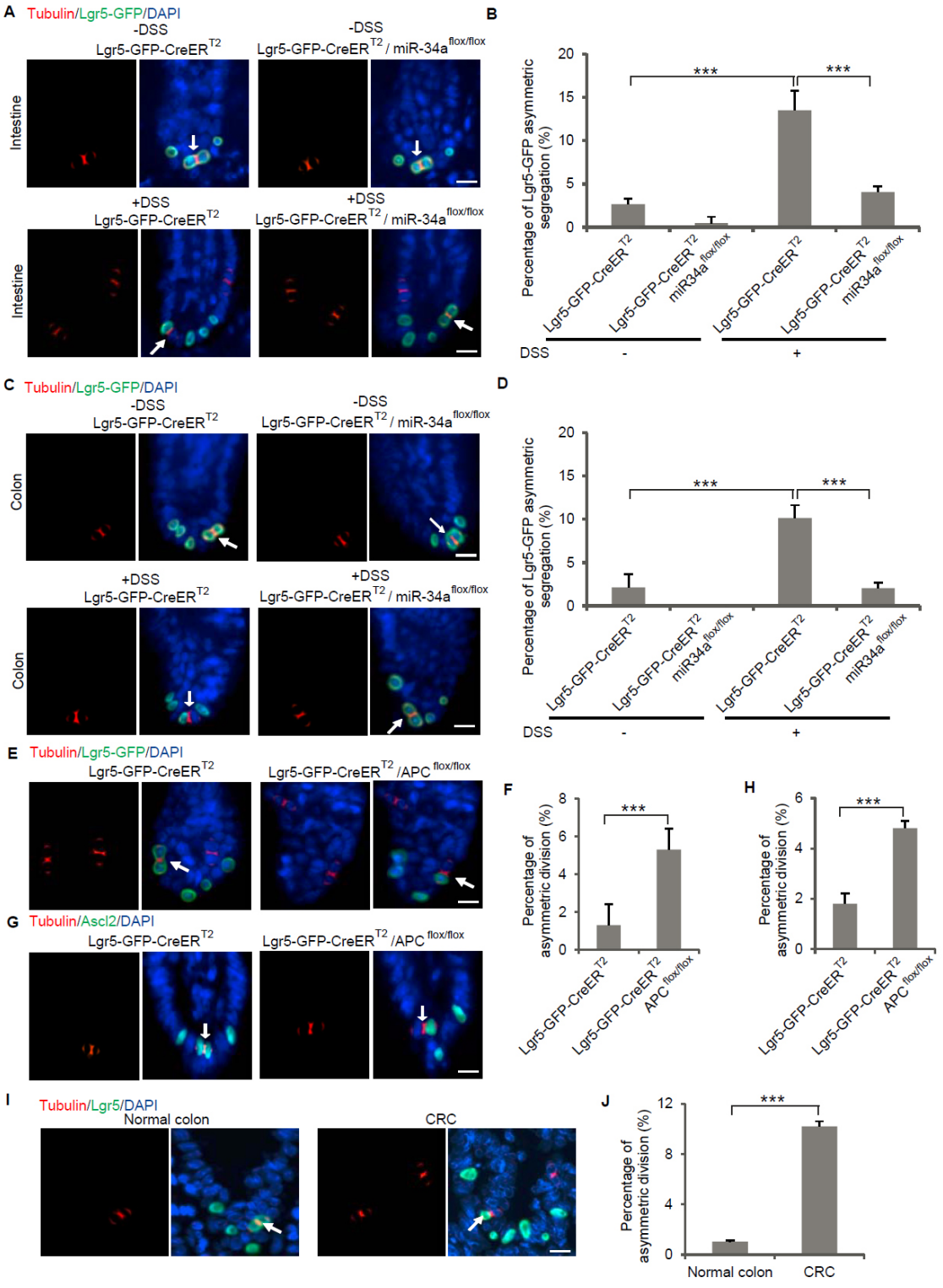

Figure S6. DSS treatment increases asymmetric division and loss-of-miR-34a abrogates asymmetric division in mouse intestine and colon. Related to Figure 7

(**A** and **B**) Representative images (A) and quantification (B) of symmetric and asymmetric division of Lgr5-GFP intestinal stem cells in *Lgr5-EGFP-CreER^{T2}* and *Lgr5-EGFP-CreERT2/miR-34a$^{flox/flox}$* mice with (+DSS) or without (-DSS) treatment. (**C** and **D**) Representative images (C) and quantification (D) of symmetric and asymmetric division of Lgr5-GFP colon stem cells in *Lgr5-EGFP-CreER^{T2}* and *Lgr5-EGFP-CreER^{T2}/miR-34a$^{flox/flox}$* mice with (+DSS) or without (-DSS) treatment. (**E** and **F**) Representative images (E) and quantification (F) of Lgr5-GFP ISC division in *Lgr5-EGFP-CreER^{T2}* mice and *Lgr5-EGFP-CreER^{T2}/APC$^{flox/flox}$* mice. (**G** and **H**) Representative images (G) and quantification (H) of Ascl2+ ISC division in *Lgr5-EGFP-CreER^{T2}* mice and *Lgr5-EGFP-CreER^{T2}/APC$^{flox/flox}$* mice. (**I** and **J**) Representative images (I) and quantification (J) of symmetric and asymmetric division of Lgr5+ cells in human normal colon and CRC tissue. Tubulin staining indicates dividing cell pair. Scale bar, 20μm. Error bars denote s.d. of triplicates. ***, $p<0.001$. p-value was calculated based on Student's t-test.

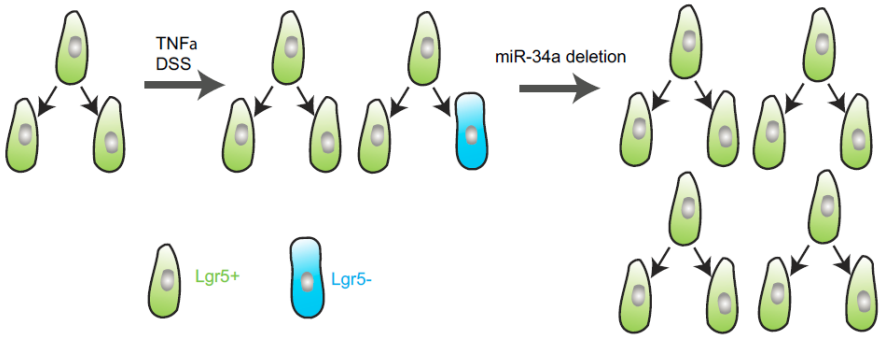

Figure S7. Schematic illustrating the effect of TNF-a/DSS treatment and miR-34a loss. Related to Figures 6 and 7.

TNFα or DSS treatment causes cell proliferation. Asymmetric division is increased to curb the number of Lgr5+ ISCs. Loss of miR-34a suppresses asymmetric division, contributing to Lgr5+ ISC proliferation.

Supplemental Experimental Procedures

Isolation and Culture of CCSCs

CCSCs were isolated and cultured as described previously (Bu et al., 2013a). Briefly, CCSCs were isolated from patient tumors by FACS based on markers CD44, CD133 and ALDH1 and functionally validated by serial sphere formation, tumor initiation, and self-renewal assays(Bu et al., 2013a). CCSCs were cultured as spheres in ultralow-attachment flasks (Corning) in DMEM/F12 (Invitrogen), supplemented with nonessential amino acids (Fisher), sodium pyruvate (Fisher), Penicillin-streptomycin (Fisher), N2 supplement (Invitrogen), B27 supplement (Invitrogen), 4 μg/mL heparin (Sigma), 40 ng/mL epidermal growth factor (Invitrogen), and 20 ng/mL basic fibroblast growth factor (Invitrogen) at 37 °C and 5% CO_2. To propagate *in vitro*, spheres were collected by gentle centrifugation, dissociated into single cells, and then cultured to form next generation spheres.

CCSC Differentiation and Sphere Formation Analysis

To induce differentiation, CCSCs were dissociated from spheres using trypsin-EDTA and were plated at 1.8×10^5 cells/mL on 60 mm dishes pre-coated with Collagen IV (Corning) in DMEM supplemented with 10% FBS and without growth factors. To measure tumor sphere formation, single CCSCs were plated in 24-well ultra-low attachment plates (Corning) at 1,000 cells per well. Tumor spheres were counted after 2 weeks in culture by an inverted microscope (Olympus).

RNA FISH

RNA FISH was performed as described as previously (Bu et al., 2013a). In brief, CCSCs were fixed with 4% formaldehyde for 30 minutes at room temperature, followed by

permeabilization in 70% ethanol at 4 °C overnight. 1-ethyl-3-(3-dimethylaminopropyl) carbodiimide (EDC) fixation was applied to prevent the loss of miRNA. After a 2 hour incubation in prehybridization buffer (25% formamide, 0.05 M EDTA, 4×SSC, 10% dextran sulfate, 1×Denhardt's solution, 0.5 mg/ml Escherichia coli tRNA and 0.5 mg/ml RVC), digoxigenin (DIG)–labeled locked nucleic acid (LNA) probe (Exiqon) was added for hybridization. The slides were then incubated with anti-DIG antibody (1:400, Roche), and the miRNA expression was detected by Rhodamine Red labeled secondary antibody (Invitrogen). DAPI (Invitrogen) was used for nucleic counterstaining. The slide was then observed under a fluorescent microscope (Olympus).

Flow Cytometry

Single CCSC sphere cells were incubated with anti-Notch1 antibody (1:100, Abcam) after fixed with formaldehyde and further permeabilized by methanol. The cells were then incubated with PE labeled secondary antibody (Invitrogen). $Notch^{high}$, $Notch^{low}$ and $Notch^{inter}$ populations were isolated by FACS using a Notch signaling reporter with tandem repeats of the RBP-Jk transcriptional response element (TRE) (Bu et al., 2013a). Lgr5-GFP population was evaluated by directly measuring GFP signal from intestinal organoids. ALDH1 levels were analyzed using the Aldeflour kit. The samples were analyzed using a BD LSR II flow cytometer. The raw FACS data were analyzed with the FlowJo software to gate cells according to their forward (FSC) and side (SSC) scatter profiles.

Quantitative Real-time RT-PCR Analysis

Total RNA was extracted from the cells using the TRIzol Reagent (Invitrogen). cDNA was synthesized from 500 ng of total RNA in 20 μl of reaction volume using the High

Capacity cDNA Archive Kit (Applied Biosystems). Quantitative PCR was carried out using the SYBR Green System (Applied Biosystems) to detect gene expression. All samples were run in triplicate three times. The primer sequences include: Notch1, 5`-GTGACTGCTCCCTCAACTTCAAT-3` and 5`-CTGTCACAGTGGCCGTCACT-3`; Notch2, 5'-AACTGTCAGACCCTGGTGAAC-3' and 5`-CGACAAGTGTAGCCTCCAATC-3`; Numb, 5`-GCTGCCTCTCCAGGTCTCTTC-3` and 5`- CGCTCTTAGACACCTCTTCTAACCA-3`; CK20, 5`-AGGAGACCAAGGCCCGTTA-3` and 5`- ATCAGTTGGGCCTCCAGAGA-3`; actin, 5`-CGCGAGAAGATGACCCAGAT-3` and 5`-ACAGCCTGGATAGCAACGTACAT-3`;. The expression of each gene was defined from the threshold cycle (Ct), and the relative expression levels were calculated using the $2^{-\Delta\Delta Ct}$ method after normalization to the actin expression level.

Western Blot

Whole cell lysate was prepared in a lysis buffer (20 mM Tris pH 7.5, 150 mM NaCl, 1% Nonidet P-40, 0.5% Sodium Deoxycholate, 1 mM EDTA, 0.1% SDS, protease inhibitors). Proteins were first separated by 10% SDS-PAGE and then transferred to a Hybond membrane (Amersham). The membranes were incubated with primary antibodies either anti-Notch1 (1:1000, Abcam), anti-Numb (1:1000, Abcam), anti-NICD (1:1000, R&D Systems), anti-Hes1 (1:500, Millipore), or anti-Action (1:1000, Abcam) in 5% milk/TBST buffer (25 mM Tris pH 7.4, 150 mM NaCl, 2.5 mM KCl, 0.1% Triton-X100) overnight, and then probed for 1 hour with secondary horseradish peroxidase (HRP)-conjugated anti-mouse or anti-rabbit IgG (Santa Cruz). After extensive wash with

PBST, the target proteins were detected on membrane by enhanced chemiluminescence (Pierce).

Lentiviral Vector Constructs and Infection

Lentiviral constructs expressing miR-34a or Numb shRNA have been described previously(Bu et al., 2013a). The Numb luciferase reporter was generated by cloning the Numb 3`UTR into the pGL3 construct. The QuickChange Site-directed Mutagenesis Kit (Stratagene) was used to mutate the miR-34a binding sequence in Numb 3`UTR. CCSCs and intestinal organoids were infected with the vectors as described previously (Bu et al., 2013a; Koo et al., 2012).

Modeling

Deterministic model

We expanded our previously published miR-34a-Notch model (Bu et al., 2013) to incorporate interactions between miR-34a, Numb, and Notch, based on microRNA regulation models from other papers (Khanin and Vinciotti, 2008; Levine et al., 2007; Mukherji et al., 2011; Osella et al., 2011; Riba et al., 2014). The ordinary differential equation (ODE) based model was used to simulate the behaviors of the IFFL:

$$\frac{d[miR34a]}{dt} = b_1 - a_1[miR34a] - r_1[miR34a][Notch_{mRNA}] - r_2[miR34a][Numb_{mRNA}]$$
$$\frac{d[Notch_{mRNA}]}{dt} = b_2 - a_2[Notch_{mRNA}] - r_1[miR34a][Notch_{mRNA}]$$
$$\frac{d[NOTCH]}{dt} = b_3[Notch_{mRNA}] - a_3[NOTCH] - r_3[NUMB][NOTCH]$$
$$\frac{d[Numb_{mRNA}]}{dt} = b_4 - a_4[Numb_{mRNA}] - r_2[miR34a][Numb_{mRNA}]$$
$$\frac{d[NUMB]}{dt} = b_5[NUMB_{mRNA}] - a_5[NUMB]$$

where

[*x*]: number of molecule of species: miR-34a, Notch mRNA, NOTCH, Numb mRNA, and NUMB

b_s: transcription/ translation rates

a_s: degradation rates

$r_{1,2}$: reaction rates of miR34a binding on $Notch_{mRNA}$ and $Numb_{mRNA}$ respectively.

r_3: reaction rate of Numb inhibition on Notch

For simplicity, the ODEs were transformed into dimensionless equations with parameters: $\tau \equiv t_0 t, miR \equiv \frac{miR34a}{miR_0}, Nm \equiv \frac{Notch_{mRNA}}{Nm_0}, N \equiv \frac{NOTCH}{N_0}, Num \equiv \frac{Numb_{mRNA}}{Num_0}, Nu \equiv \frac{NUMB}{Nu_0}, miR_0 \equiv Num_0 \equiv Nm_0$

The new dimensionless ODEs are shown as:

$$\frac{d[miR34a]}{d\tau} = \beta_1 - \alpha_1[miR34a] - \gamma_1[miR34a][Notch_{mRNA}] - \gamma_2[miR34a][Numb_{mRNA}]$$
$$\frac{d[Notch_{mRNA}]}{d\tau} = \beta_2 - \alpha_2[Notch_{mRNA}] - \gamma_1[miR34a][Notch_{mRNA}]$$
$$\frac{d[NOTCH]}{d\tau} = \beta_3[Notch_{mRNA}] - \alpha_3[NOTCH] - \gamma_3[NUMB][NOTCH]$$
$$\frac{d[Numb_{mRNA}]}{d\tau} = \beta_4 - \alpha_4[Numb_{mRNA}] - \gamma_2[miR34a][Numb_{mRNA}]$$
$$\frac{d[NUMB]}{d\tau} = \beta_5[NUMB_{mRNA}] - \alpha_5[NUMB]$$

where $\beta_1 \equiv \frac{b_1}{miR_0 t_0}, \beta_2 \equiv \frac{b_2}{Nm_0 t_0}, \beta_3 \equiv \frac{b_3 Nm_0}{N_0 t_0}, \beta_4 \equiv \frac{b_4}{Num_0 t_0}, \beta_5 \equiv \frac{b_5 Num_0}{Nu_0 t_0}, \alpha_1 \equiv \frac{a_1}{t_0}, \alpha_2 \equiv \frac{a_2}{t_0}, \alpha_3 \equiv \frac{a_3}{t_0}, \alpha_4 \equiv \frac{a_4}{t_0}, \alpha_5 \equiv \frac{a_5}{t_0}, \gamma_1 \equiv \frac{r_1 miR_0}{t_0}, \gamma_2 \equiv \frac{r_2 miR_0}{t_0}, \gamma_3 \equiv \frac{r_3 Nu_0}{t_0}$

Parameter values used for Fig. 2d:

- IFFL: β_1= various, β_2= 360, β_3= 0.0112, β_4= 400, β_5= 0.0008, α_1= 0.002, α_2= 0.027, α_3= 0.02, α_4= 0.009, α_5= 0.002, γ_1= $6x10^{-5}$, γ_2= $2x10^{-5}$, γ_3= 10^{-5}
- NumbKD: β_1= various, β_2= 0.018, β_3= 29.38, α_1= 0.4, α_2= 0.027, α_3= 0.002, γ_1= $6x10^{-5}$

Parameter values used for Supplemental Fig. S2:

- β_1= various, β_2= 360, β_3= 0.0112, β_4= 400, β_5= 0.0008, α_1= 0.002, α_2= 0.027, α_3= 0.02, α_4= 0.009, α_5= 0.002, γ_1= [$4.2x10^{-6}$~$2.4x10^{-4}$], γ_2= [$4x10^{-6}$~$2.8x10^{-5}$], γ_3= 10^{-5}

Stochastic simulation

Stochastic simulations were performed using the stochastic solver, stochastic simulation algorithm (SSA), in the Matlab (MathWork®) toolbox SimBology with the reactions listed below:

Reaction	Parameter
1. Transcription of miR-34a	b_1
2. Degradation of miR-34a	a_1
3. miR-34a binding on Notch mRNA	r_1
4. miR-34a binding on Numb mRNA	r_2
5. Transcription of Notch mRNA	b_2
6. Degradation of Notch mRNA	a_2
7. Translation of Notch	b_3
8. Degradation of Notch	a_3
9. Transcription of Numb mRNA	b_4
10. Degradation of Numb mRNA	a_4

11. Translation of Numb b_5
12. Degradation of Numb a_5
13. Numb inhibition on Notch r_3

Based on previous FACS measurement of induced miR-34a(Bu et al., 2013), we applied a stochastic transfer function $f(x) = kx(1 \pm \xi\%)$ to model miR-34a induction, where x refers to the number of molecules, k refers to the signal intensity coefficient, and ξ denotes the variation of signal intensity. Stochastic simulations were run to reach steady states determined by deterministic simulations, and levels were sampled at the same time point for statistics.

Parameter values used for Fig. 2e:

- IFFL: b_1= various, b_2= 360, b_3= 0.0112, b_4= 400, b_5= 0.0008, a_1= 0.002, a_2= 0.027, a_3= 0.02, a_4= 0.009, a_5= 0.002, r_1=6x10^{-5}, r_2= 2x10^{-5}, r_3= 1x10^{-5}, k= 1, ξ= 20
- NUMB KD: b_1= various, b_2= 1.8, b_3= 0.0113, a_1= 0.002, a_2= 0.027, a_3= 0.02, r_1= 6x10^{-5}, k= 1, ξ= 20

Supplemental References

Khanin, R., and Vinciotti, V. (2008). Computational modeling of post-transcriptional gene regulation by microRNAs. J Comput Biol *15*, 305-316.

Levine, E., Ben Jacob, E., and Levine, H. (2007). Target-specific and global effectors in gene regulation by MicroRNA. Biophys J *93*, L52-54.

Mukherji, S., Ebert, M.S., Zheng, G.X., Tsang, J.S., Sharp, P.A., and van Oudenaarden, A. (2011). MicroRNAs can generate thresholds in target gene expression. Nature genetics *43*, 854-859.

Osella, M., Bosia, C., Cora, D., and Caselle, M. (2011). The role of incoherent microRNA-mediated feedforward loops in noise buffering. PLoS Comput Biol *7*, e1001101.

Riba, A., Bosia, C., El Baroudi, M., Ollino, L., and Caselle, M. (2014). A combination of transcriptional and microRNA regulation improves the stability of the relative concentrations of target genes. PLoS Comput Biol *10*, e1003490.